



Empirical ground-motion models (GMMs) and associated correlations for cumulative absolute velocity, Arias intensity, and significant durations calibrated on Iranian strong motion database

Mehran Davatgari-Tafreshi¹ · Sanjay Singh Bora²

Received: 11 November 2022 / Accepted: 9 May 2023 / Published online: 19 May 2023
© The Author(s), under exclusive licence to Springer Nature B.V. 2023

Abstract

This study presents empirical ground-motion models (GMMs) for estimating Arias intensity (I_A), cumulative absolute velocity (CAV) and significant ground-motion duration (D_{5-75} and D_{5-95}), calibrated on Iranian strong motion database. The dataset consists of 1749 (with two horizontal components) acceleration motion time-series originated from 566 events with moment magnitude (M_w) 3–7.5 range and recorded at 338 stations in the distances range up to 200 km. Common functional forms were adopted for all four models to facilitate easy comparison of derived model parameters and model predictions. Residual distributions and their unbiased variation with predictor variables M_w , hypocentral distance (R_{hypo}), time-averaged shear-wave velocity in the top 30 m (V_{S30}) indicated robustness of the derived models. This study also examines residual correlations between different pairs of ground-motion intensity measures (GMIMs). The correlations were analysed separately for between-event (δB_e) and within-event (δWS_{es}) component of the residuals. The correlation of δB_e between: (1) I_A and the two duration measures (D_{5-75} and D_{5-95}), (2) CAV and the two duration measures were found depending upon the event magnitude (strongest for $M_w > 6$). Similarly, the correlation of δWS_{es} between: (1) I_A and the two duration measures, (2) CAV and the two duration measures were observed depending upon source-to-site distance (strongest for $R_{\text{hypo}} < 50$ km). Furthermore, a relatively stronger negative correlation of δWS_{es} was observed between CAV and station-specific attenuation parameter (κ_0) (mainly at softer soil sites) in comparison to that between I_A and κ_0 .

Keywords Ground-motion models · Duration · Arias intensity · Cumulative absolute velocity · Correlations · Iranian plateau

✉ Mehran Davatgari-Tafreshi
mdvtgrtf@memphis.edu

¹ Department of Civil Engineering, The University of Memphis, Memphis, TN 38152, USA

² Institute of Geological and Nuclear Science (GNS), Lower Hutt, New Zealand

1 Introduction

A reliable estimation of ground motions that can be produced by future earthquakes is an essential element of any seismic hazard analysis study. This is achieved by employing empirically derived ground motion models (GMMs) that provide a conditional distribution of expected ground motion as a function of magnitude, distance, and site condition. Often, probabilistic seismic hazard analysis (PSHA) and probabilistic seismic risk analysis (PSRA) consider elastic response spectral ordinates as the primary ground motion intensity measures (GMIMs) and the GMIMs are conventionally used as a single ground-motion measure. However, it is widely acknowledged that a single measure of GMIM may not fully capture all the aspects of the ground shaking that are of engineering interest (Shome et al. 1998; Luco and Cornell 2007). A vector of GMIMs is widely applied in several applications such as probabilistic seismic risk analysis and multi-GMIM based ground-motion selections (Bradley 2011a; Du et al. 2020). Also, for vector-valued probabilistic seismic hazard and risk analysis (Baker 2007; Huang and Zhang 2021) a vector of GMIMs is recommended.

In this context, Arias intensity (I_A), cumulative absolute velocity (CAV) and significant duration (SD) are often considered as additional GMIMs that characterize various aspects of strong ground motions that are of engineering importance. Thus, recently, various studies have proposed empirical models for significant durations (Kempton and Stewart 2006; Bommer et al. 2009; Yaghmaei-Sabegh et al. 2014; Afshari and Stewart 2016; Sandikkaya and Akkar 2017; Du and Wang 2017; Baharampouri et al. 2020; Meimandi-Parizi et al. 2020). The ground-motion models for durations are also used to obtain response spectral ordinates along with empirical Fourier models (Vanmarcke and Lai 1980; Reinoso et al. 1990; Jaimes et al. 2006; Bora et al. 2014). Moreover, ground-motion duration is an essential element of stochastic simulations (Boore 2003; Boore and Thompson 2014; Kolli and Bora 2021). When compared to the GMMs of elastic response spectrum, the published ground-motion models for cumulative measures of ground-motion I_A and CAV are rather limited (Douglas 2012). Most of the existing I_A and CAV GMMs have been developed for active crustal tectonic regions (Campbell and Bozorgnia 2010, 2012, 2019; Du and Wang 2012; Foulser-Piggott and Goda 2015; Macedo et al. 2020). Since CAV models have a lower standard deviation as compared to the other GMIMs, they can be implemented to wider range of engineering applications (Campbell and Bozorgnia 2012). Recent studies (Stafford et al. 2009; Campbell and Bozorgnia 2010, 2012; Lee et al. 2012; Bustos and Stafford 2012; Foulser-Piggott and Stafford 2012; Du and Wang 2012; Du and Wang 2013; Foulser-Piggott and Goda 2015; Abrahamson et al. 2016; Sandikkaya and Akkar 2017; Campbell and Bozorgnia 2019; Macedo et al. 2019; Macedo et al. 2020; Bahamrampouri et al. 2020; Farhadi and Pezeshk 2020) have proposed empirical models for cumulative measures of ground motion, I_A and CAV.

The generalized conditional intensity measures approach of Bradley (2010) provides a probabilistic framework in which a combination of GMIMs can be considered in ground-motion selection. A key component of this probabilistic framework is the availability of the correlation between various GMIMs. Many correlation models have been developed, including the correlations for spectral accelerations at different vibration periods (Goda 2011; Cimellaro 2013), spectral accelerations and spectral intensities (Bradley 2011a), significant duration and cumulative GMIMs (Bradley 2011b), peak ground velocity (PGV) and spectrum-based GMIMs (Bradley 2012), Arias intensity (I_A) and amplitude, duration, and cumulative GMIMs (Bradley 2015; Du 2019), spectral input energy at different

vibration periods (Cheng et al. 2020) and empirical correlations of spectral input energy with peak amplitude, cumulative, and duration intensity measures (Cheng et al. 2022).

In the context of Iran, researchers have mainly focused on developing GMMs for predicting amplitude-based and spectrum-based GMIMs, such as PGA and spectral pseudo-acceleration (PSA) (Sedaghati and Pezeshk 2017; Zafarani et al. 2018; Darzi et al. 2019; Farajpour et al. 2019). These GMIMs (PGA and PSA based) describe ground motion amplitude and frequency content but fail to capture the cumulative effect of ground motion duration and intensity (Farhadi and Pezeshk 2020). Yaghmaei-Sabegh et al. (2014) and Meimandi-Parizi et al. (2020) duration models (D_{5-75} and D_{5-95}) are calibrated on earlier versions of Iranian strong motion database. As mentioned earlier, cumulative-based GMIMs, in particular, I_A and CAV, could be used in line with amplitude-based and spectrum-based GMIMs to characterize strong ground motion fully for engineering applications. To the best of our knowledge, there are no studies available in literature that are focussed on developing models for cumulative intensity measures such as I_A and CAV in addition to their correlations with other GMIMs. This warrants the need for developing empirical models for duration-related and cumulative-based GMIMs such as I_A , CAV, and significant durations, importantly, to quantify and understand the associated correlation between various GMIMs.

In the present study, we develop empirical models for Arias Intensity (I_A), Cumulative Absolute Velocity (CAV), and significant strong-motion duration (D_{5-75} , D_{5-95}) calibrated on Iranian strong motion database. The major objective of this study is to investigate correlation between different pairs of GMIMs in addition to investigating the variability in these GMIMs for the selected dataset. For that purpose, a common functional form is deemed to be appropriate for all the four GMIMs which is further verified by residuals variation and comparison (of median predictions) with other regional and global models. The correlation between different pairs of GMIMs is presented by computing residual correlations (Bradley 2011b, 2015) separately for between-event and within-event components which were subsequently combined to present the correlations of total residuals. This article is organized as follows: (1) definitions of the GMIMs used in this study, (2) summary of the strong ground-motion dataset, (3) calibration of empirical models for significant durations (D_{5-75} , D_{5-95}), I_A and CAV, and (4) investigation of residual correlations.

2 I_A , CAV and significant durations

Arias Intensity (I_A) is a duration related GMIM that represents the total earthquake input energy per unit weight for a set of un-damped elastic oscillators with frequencies uniformly distributed from zero to infinity (Arias 1970).

$$I_A = \frac{\pi}{2g} \int_0^T (a(t))^2 dt \quad (1)$$

where $a(t)$ is the ground acceleration in m/s^2 , g is the gravitational acceleration, T is the total duration of the ground motion recording and I_A is the Arias Intensity in m/s . I_A combines amplitude and duration and has been considered as a useful indicator of damage potential for earth dams in seismic analysis (Travasarou et al. 2003). Several studies have found that I_A correlates well with distributions of earthquake-induced landslides (Harp and Wilson 1995; Keefer 2002) and building damage (Cabanias et al. 1997).

Cumulative Absolute Velocity (CAV) is a scalar GMIM, and it is originally defined as the total area under the absolute ground acceleration ($a(t)$) with total duration:

$$CAV = \int_0^T |a(t)| dt \quad (2)$$

where $a(t)$ is the acceleration at time t (in unit of m/s^2), T is the duration of time series. One can draw a more intuitive interpretation of CAV as the product of total absolute acceleration and duration of the acceleration trace. The term velocity in CAV essentially reflects integration of acceleration with respect to time. Several studies used CAV for: distinguishing between potentially damaging ground motions in the high frequency range and non-damaging ground motion (EPRI 1998), formulate the generation of excessive pore water pressure for potentially liquefiable soils, peak displacements of pile foundations under seismic loading (Kramer and Mitchel 2006; Bradley et al. 2009), soil structure interaction problem (Macedo 2017; Bray and Macedo 2017; Bullock et al. 2019a; b; Azizi et al. 2022; Kashani et al. 2022), structural analyses and time-history selection (Muin and Mosalam 2017; Danciu and Tselentis 2007; Tarbali et al. 2019), seismic risk analysis of critical facilities and, in the context of earthquake early warning system (Fahjah et al. 2011). After EPRI (1998) study, CAV was used as a scalar intensity measure that combines both the amplitude and duration. Usually, I_A and CAV are considered as crucial GMIMs, for engineering applications, because they reflect more than one key aspect of the strong ground motion at the same time, and the key advantage of them over peak response parameters is evident from their mathematical expressions in Eqs. (1) and (2).

There is no consensus on the definition of strong ground-motion duration in literature. Often, a particular definition is driven by application. From engineering application perspective, a detailed review of strong ground-motion duration definitions and on their measurement methods can be found in Boomer and Martinez-Pereir (1999). In this study, we use significant duration definitions as the measure of strong ground-motion duration. It uses husid plots to compute the time elapsed between different levels of cumulative I_A (Arias 1970). D_{5-75} and D_{5-95} considers the time interval between 5 and 75%, and 5–95% of the normalized cumulative I_A . D_{5-75} is intended to capture the energy from the body waves, whereas the D_{5-95} includes a large portion of the full waveform (Meimandi-Parizi et al. 2020) that often includes low frequency surface waves and coda (Bommer et al. 2009). Figure 1 demonstrates the computation of significant durations (D_{5-75} and D_{5-95}) from an acceleration time history of the 2019/11/07 earthquake used in this study.

It is worth mentioning that in core seismological studies such as in numerical simulations of realistic waveforms, the duration is related with the slip rise-time at a particular point and for larger events it also includes effect of finiteness of the fault through rupture velocity (Boore 2003).

In engineering applications, various studies have highlighted the importance of strong ground-motion duration (e.g., Rauch and Martin 2000; Chai et al. 1998; Tiwari and Gupta 2000; Krawinkler et al. 1983; Seed and Idriss 1982; Hancock and Bommer 2006). It has been shown that significant durations (D_{5-75} and D_{5-95}) correlate well with structural damage and can be used in both geotechnical earthquake engineering as well as in record selection (Boomer et al. 2009; Bradley 2011b; Lee and Green 2014). Also, significant durations have been used for structural damage assessment (Chai et al. 1998; Bommer et al. 2004; Iervolino et al. 2006; Ruiz-Garcia 2010; Chandra Mohan et al. 2016). Tremblay (1998) as well as Hou and Qu (2015) consider strong motion duration for generating realistic stochastic simulations. Recently, Kolli and Bora (2021) have investigated the use of significant

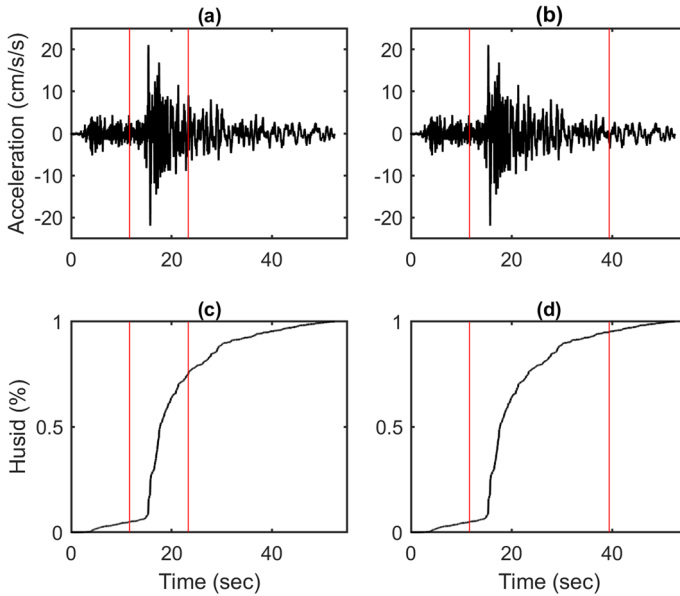


Fig. 1 Plots showing the significant duration from the acceleration time series (H1 component) of the 2019/11/07 earthquake with M_w 5.9 recorded at Basmanj station. Upper panels (a and b) depict the selected significant duration based on the time interval between (a) the 5% and 75% and (b) the 5% and 95% levels of the normalized Arias intensity (Arias 1970) (bottom panels c and d)

durations (D_{5-75} and D_{5-95}) for generating response spectra using empirical models for Fourier amplitude spectrum (FAS).

3 Dataset and processing of strong motion records

We used 1749 three-component acceleration time histories from 566 events that were recorded by 338 stations from 1976 to 2020. The data is taken from the Building and Housing Research Center (BHRC) of Iran. In the Iranian plateau, collection of strong motion data often faces challenges particularly with regard to metadata information of the records such as site-characterization of strong motion station sites, focal mechanism and event-depths for large events. The raw acceleration traces obtained from BHRC website were fully processed by us using standard signal processing protocols suggested by Boore and Akkar (2003), Boore (2005), Boore and Bommer (2005). The major processing steps we followed for processing of strong motion records are summarized in what follows.

We rotated longitudinal and transverse components to obtain the two orthogonal horizontal components North-South (H1) and East-West (H2) components. We also performed the base line corrections that includes removing the mean and de-trending any linear trend in the raw acceleration records.

The orientation-independent component is calculated using the scheme suggested by Boore (2010), and the two as-recorded orthogonal components (H1 and H2) are combined into a single time series and is rotated between orientations of 0° and 180° (Boore 2010) as follows:

$$H_{ROT}(t;\theta) = H_1(t)\cos(\theta) + H_2(t)\sin(\theta) \tag{3}$$

This procedure is for finding RotD50 (the 50th percentile of the rotated orientation-independent) PSA. Similarly, an orientation-independent RotD50 values for D_{5-75} , D_{5-95} , I_A and CAV (from two orthogonal components H1 and H2) are computed in this study.

The final processed dataset consists of recordings made from earthquakes in the magnitude range M_w 3–7.5 at distances from 10 up to 200 km. We only used crustal events with hypocentral depth up to 50 km. The magnitude-distance distribution of events is shown in Fig. 2a. In the compiled dataset we have considered stations which have recorded at least three events, and events were recorded by at least three stations. Figures 2b and c show histograms of the data in different magnitude and distance bins, respectively. Figure 2d shows distribution of the measured V_{S30} values in the selected dataset.

In our dataset, the event magnitude scale is not homogenous and some of the events are reported with Nuttli magnitude scales (M_N), local magnitude scale (M_L), and body-wave magnitude scale (m_b). In order to have a uniform magnitude scale, we converted different magnitude types to a uniform M_w scale. The magnitude scale conversion is performed using the empirical relationships developed by Mousavi and Babaie Mahani (2020) for the Iranian Plateau (for more details, the reader is referred to Davatgari-Tafreshi et al. 2021 and Davatgari-Tafreshi et al. 2022).

4 Functional form and regression analysis

In this section, we derive empirical GMMs for I_A , CAV and significant durations (D_{5-75} , D_{5-95}) calibrated on the Iranian strong motion database. We adopt a common functional form for all the four GMIMs to facilitate easy comparison between the model predictions

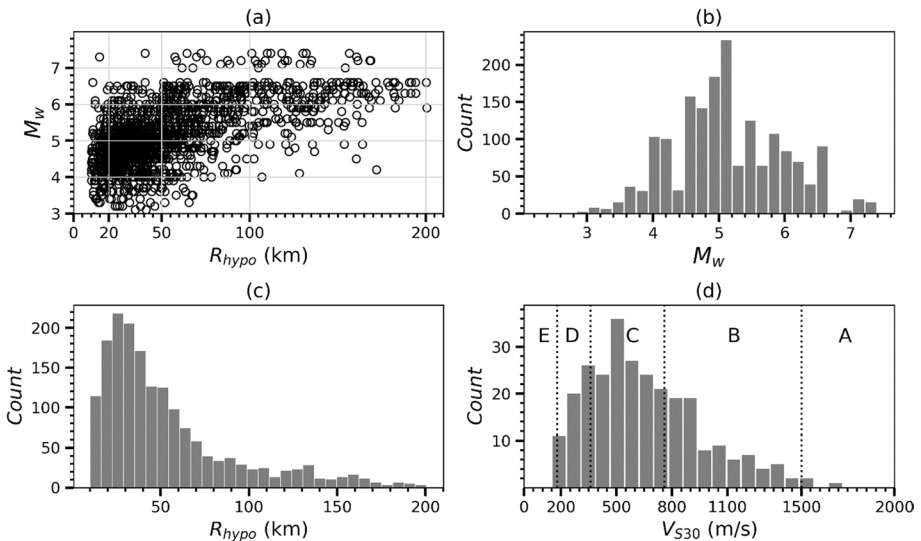


Fig. 2 a Magnitude-distance distribution, b Magnitude (M_w) histograms, c distance (R_{hypo}) histograms, and d V_{S30} histogram for the selected database. Vertical dashed lines depict the limits of National Earthquake Hazard Reduction Program (NEHRP) site classes (E: Soft soil; D: Stiff soil; C: Very dense soil and soft rock; B: Rock; A: Hard rock)

and associated coefficients. However, the final judgement on the adopted functional-form was made by investigating residual variation and associated aleatory uncertainty. The functional dependence over predictor variables such as magnitude, source-to-site distance (hypocentral distance) and site V_{S30} involves similar functional dependence to that of empirical models for peak-amplitudes and spectral ordinates (e.g., PSA). The primary motive of choosing such a functional dependence was to facilitate easy interpretation of regressed coefficients with respect to their counterparts in response spectral and Fourier domain. However, as noted earlier, I_A and CAV are expected to capture combined effect of both amplitude and duration information from a recorded trace. Similarly, the significant duration measures used in the current study capture source duration (i.e., size of the event) and propagation effects related to dispersion and scattering of seismic waves. In order to select a functional form for all models, many preliminary regression and visual checks were performed. The final functional form considered as:

$$Y = c_1 + F_e(M_w) + F_p(R_{hyp}, M_w) + F_s(V_{S30}) + \delta B_e + \delta WS_{es} \tag{4}$$

where Y represent the natural log of either I_A , CAV, D_{5-75} and D_{5-95} with respective units; δB_e and δWS_{es} represent between-event and within-event residual respectively (Al Atik et al. 2010). The predictor variables are the moment magnitude (M_w), hypocentral distance (R_{hyp}) and V_{S30} (time-averaged shear-wave velocity in upper 30 m of the soil column). We adopt a linear site-response term as a simple function of V_{S30} . We also tested other forms of site response function (more complex) and nonlinear site behaviour in our models. One reason for not being able to incorporate nonlinear site behaviour could be insufficient soft-site recordings at short distances. This is further validated by the variation of residuals as a function of V_{S30} discussed later. The source (F_e), path (F_p) and site (F_s) functions are described as follows:

The source (event) function F_e is given by the following equation:

$$F_e = c_2(M_w - 6.5) + c_3(8.5 - M_w)^2 \tag{5}$$

The path function F_p is given by:

$$F_p = [c_4 + c_5(M_w - 6.5)] \ln\left(\sqrt{R_{hyp}^2 + c_6^2}\right) \tag{6}$$

The site function F_s is given by:

$$F_s = c_7 \ln(V_{S30}) \tag{7}$$

The model parameters (i.e. coefficients, c_1 - c_7) of our four empirical models in Eqs. (4–7), were determined using mixed effects regression algorithm (Bates et al. 2015) separately for D_{5-75} , D_{5-95} , I_A and CAV. This regression algorithm allows decomposition of total residuals into between-event component (δB_e) with zero mean and standard deviation τ and within-event residual (δWS_{es}) with zero mean and standard deviation ϕ . The model coefficient c_6 (pseudo-depth term) was derived in the first step by performing a simple non-linear regression (fully fixed-effects regression). The remaining model coefficients and the between-event and within-event standard residuals were derived using linear mixed-effects regression (Bates et al. 2015), keeping c_6 as the value determined from the previous stage. Note that the decomposition of residuals and estimation of model coefficients is performed together in a single step.

The final coefficients (for significant duration (D_{5-75} and D_{5-95}), I_A , and CAV models) along with corresponding standard errors in parameter estimations and statistical p -values are presented in Tables 1 and 2. We observe from Table 1 (for D_{5-75} and D_{5-95}) that a large standard-error is associated with estimation of coefficients c_3 and c_5 which results in a large p -value (statistical insignificance). It clearly suggests that both, a quadratic dependence over magnitude and a magnitude-dependent distance scaling of D_{5-75} and D_{5-95} cannot be resolved by using the current dataset as observed by other studies (Sandikkaya and Akkar 2017; Bora et al. 2019). For I_A and CAV models, all coefficients are found statistically significant (Table 2). The full variance-covariance matrices of estimated coefficients for all four models are presented in supplementary material (Table S1- Table S4). Note that the magnitude range covered by the present dataset is between M_W 3.0–7.5 however, based on residual variations and comparison of median predictions with other global models we consider these models to be valid for events between M_W 4.0–7.0 in the distance range 20–200 km. An extrapolation of the models beyond the magnitude and distance range prescribed here must be validated vis-à-vis observed ground motions and with proper caution, if required. In the following sections, we first discuss comparison of the median

Table 1 Coefficients associated with D_{5-75} and D_{5-95} models from mixed effects regression

Coeff	D_{5-75} model	SE	p -value	D_{5-95} model	SE	p -value
C_1	2.8167	0.32497	1.26e−17	3.7857	0.22245	7.38e−60
C_2	0.76957	0.29872	0.019809	0.49642	0.21201	0.019326
C_3	−0.0026668	0.027755	0.85988	−0.014058	0.02052	0.49339
C_4	0.29208	0.059882	8.31e−07	0.21296	0.040659	1.83e−07
C_5	−0.086243	0.039605	0.069937	−0.064478	0.027296	0.018286
C_6	4.402	0.3434	0.0011	3.275	0.2192	0.00087
C_7	−0.27425	0.034212	2.05e−15	−0.26241	0.023416	4.02e−28
τ	0.1556	–	–	0.1612	–	–
ϕ	0.5633	–	–	0.3649	–	–
σ	0.5844	–	–	0.3990	–	–

Table 2 Coefficients associated with I_A and CAV models from mixed effects regression

Coeff	I_A model	SE	p -value	CAV model	SE	p -value
C_1	7.83	0.53402	8.66e−46	6.7445	0.25396	3.28e−129
C_2	7.3383	0.53193	5.24e−41	3.972	0.25998	2.55e−49
C_3	0.40319	0.052092	1.743e−14	0.19804	0.026032	4.71e−14
C_4	−2.6671	0.098303	7.65e−134	−1.2697	0.0465	2.96e−135
C_5	−0.75652	0.068859	3.95e−27	−0.4213	0.033036	1.48e−35
C_6	7.395	0.486	0.0012	8.052	0.238	0.000197
C_7	−0.28514	0.054923	2.34e−07	−0.25831	0.026044	1.51e−22
τ	0.5087	–	–	0.2825	–	–
ϕ	0.8176	–	–	0.3776	–	–
σ	0.9630	–	–	0.4716	–	–

† SE: Standard error of the coefficients

† p -value: p -value for the t -statistic of the two-sided hypothesis test. If the p -value of the t -statistic for a coefficient is greater than 0.05, this term is not significant at the 5% significance level given the other terms in the model.

predictions from the four empirical models with other regional and global studies. Following that, we discuss the residual variations. Finally, residual-correlations between different pairs of GMIMs are presented.

5 Median predictions

In this section we present comparisons of the median predictions from the empirical models derived in this study with those from recently published models. The comparisons for significant durations are performed with Meimandi-Parizi et al. (2020) (hereafter MPA20), Yaghmaei-Sabegh et al. (2014) (hereafter YSS14), Afshari and Stewart (2016) (hereafter AS16) and Sandikkaya and Akkar (2017) (hereafter SA17) studies. The MPA20 and YSS14 models are calibrated on earlier versions of Iranian strong motion database whereas AS16 represents a global model calibrated on NGA-West2 (Ancheta et al. 2014) database with most of the records obtained from California region. Similarly, SA17 models for SD are calibrated on a pan-European (RESORCE) strong motion database (Akkar et al. 2014) with records dominated from Turkey and Italy. SA17 and AS16 used R_{hypo} and R_{rup} in their models, respectively. Figures 3, and 4 depict comparison of median predictions as

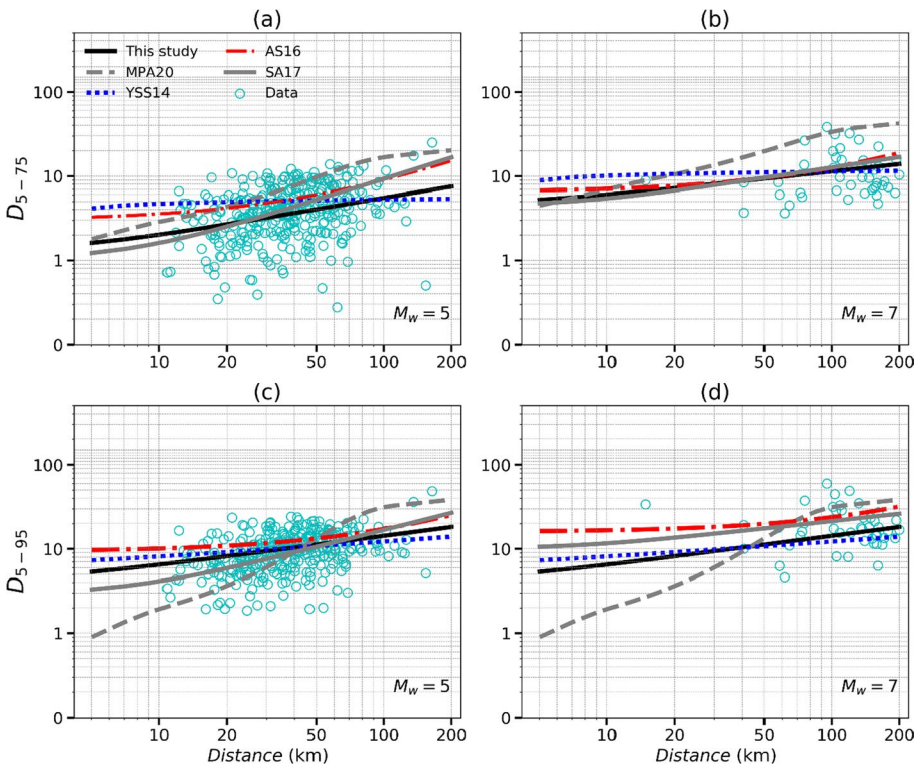


Fig. 3 Comparisons of distance scaling for the D_{5-75} (a and b) and D_{5-95} (c and d) significant duration models (median duration values) derived in this study, and models from previous studies (MPA20, YSS14, AS16 and SA17) for $V_{S30}=800$ m/s. Note that, the AS16, SA17 and MPA20 predictions are shown for strike-slip events. Cyan empty circles are the observed strong-motion data

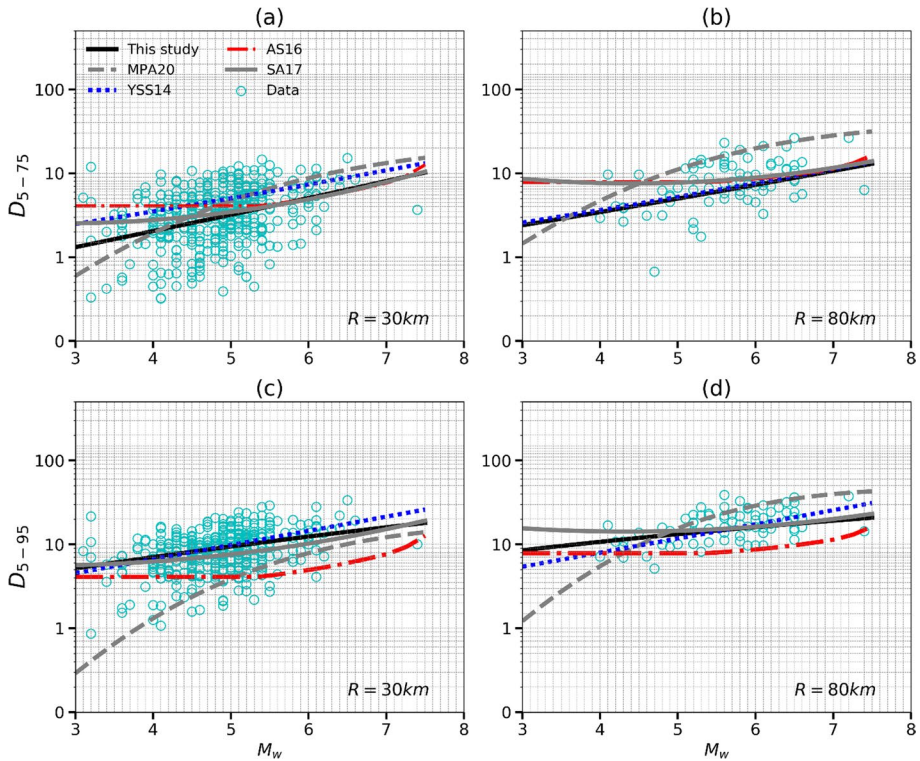


Fig. 4 Comparisons of magnitude scaling for the D_{5-75} (a and b) and D_{5-95} (c and d) significant duration values (median duration values) derived in this study, and models from previous studies (MPA20, YSS14, AS16 and SA17) for $V_{S30}=800$ m/s. Note that, the AS16, SA17 and MPA20 predictions are shown for strike-slip events. Cyan empty circles are the observed strong-motion data

a function of distance and magnitude, respectively. The differences in median predictions between different models are usually due to differences in underlying datasets and differences in functional dependence over magnitude, distance and V_{S30} . The differences may also stem from incomplete functional forms that overlook, for example, the differences in stress drop, anelastic attenuation, and geometrical spreading. Thus, as expected there are differences in absolute values of D_{5-75} and D_{5-95} between the median predictions but, in general the distance scaling is consistent with the global model of AS16 and the pan-European model of SA17. The distance scaling of MPA20 is slightly different at larger distance which is mainly due to a different functional form adopted in their study. Median predictions from YSS14 model are in general good agreement with those from current study except with minor differences at shorter distances for smaller magnitude events. Note that the YSS14 model adopts a different functional dependence over magnitude and distance and that it uses base 10 of logarithm. For magnitude scaling of D_{5-75} and D_{5-95} , the predictions from this study are in general good agreement with AS16 and SA17. The differences in the shape of the scaling are due to functional form, distance metric used, and actual differences in the underlying scaling of the ground motion with magnitude and/or distance. The last point is important where the functional form and distance metrics are identical for example the differences with SA17. In this case, the differences are due to differences in

the underlying datasets. The D_{5-75} values from MPA20 are slightly larger than those from current study. Particularly, the magnitude scaling (i.e., slope) of MPA20 at smaller magnitudes is relatively stronger than that from other models. We observe an identical magnitude scaling of D_{5-75} from our model with that of AS16 and SA17 at $M_w > 5$. Note that the functional dependence of significant durations of AS16 is derived from seismological theory where the source component of ground-motion duration is considered as the reciprocal of Brune’s (1970, 1971) source corner frequency. The larger difference in scaling for D_{5-95} is mainly due to that a quadratic magnitude scaling of significant durations cannot be resolved by the current dataset as mentioned earlier (see Table 1). It is worth mentioning here that with NGA-West2 database that covers a much broader magnitude range AS16 and Bora et al. (2019) have found a rather weak dependence of duration over magnitude below $M_w < \sim 5$.

Median predictions of I_A and CAV are compared with recently derived I_A and CAV models from SA17. As noted earlier, the I_A and CAV models of SA17 are calibrated on a pan-European strong motion database. Figures 5 and 6 show comparison of median predictions for I_A and CAV as a function of distance and magnitude, respectively. Figure 5 clearly demonstrates that I_A scales rather strongly with distance in comparison to CAV.

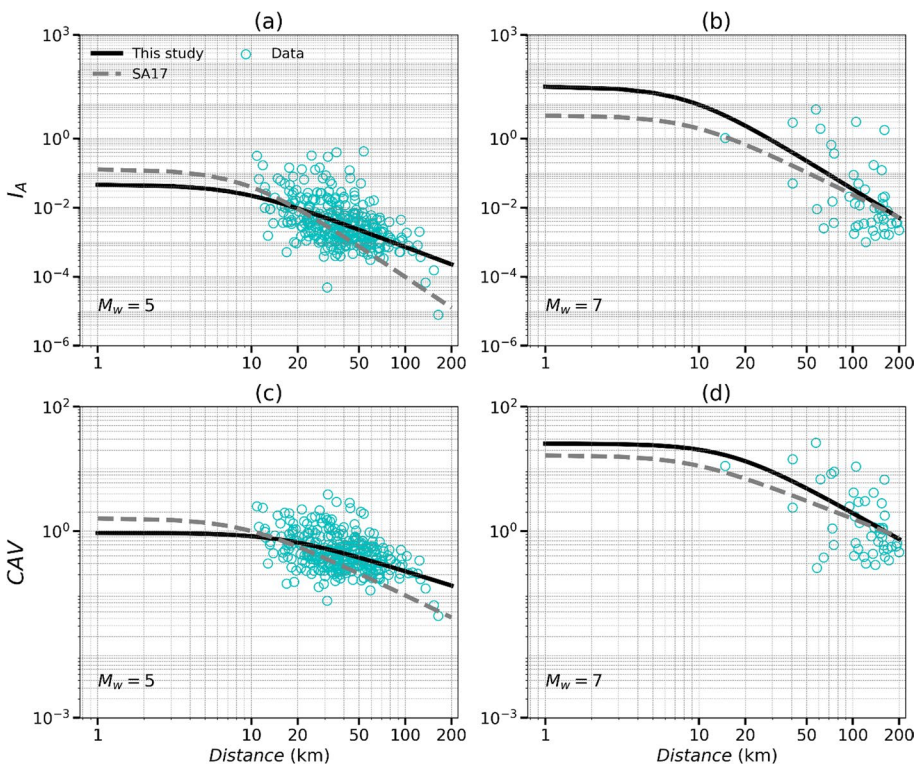


Fig. 5 Comparisons of distance scaling for the I_A and CAV models (median I_A and CAV values) derived in this study, and models from previous study (SA17) for $V_{S30}=800$ m/s. Note that the SA17 predictions are shown for strike-slip events and extrapolated for $M_w < 4$. Cyan empty circles are the observed strong-motion data in the selected magnitude ($4.8 < M_w < 5.2$ and $6.6 < M_w < 7.4$) and V_{S30} ($600 < V_{S30} < 1000$ m/s) bins

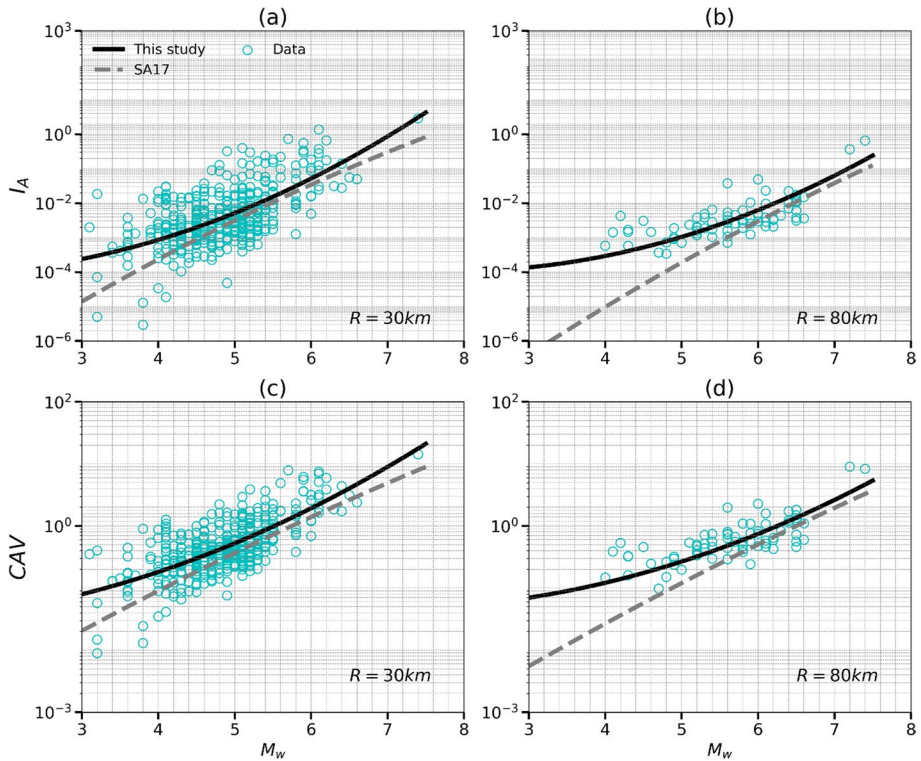


Fig. 6 Comparisons of magnitude scaling for the I_A and CAV models (median I_A and CAV values) derived in this study, and models from previous study (SA17) for $V_{S30}=800$ m/s. Note that the SA17 predictions are shown for strike-slip events and extrapolated for $M_w < 4$. Cyan empty circles are the observed strong-motion data in selected distance ($20 < R < 40$ and $70 < R < 90$ km) and V_{S30} ($600 < V_{S30} < 1000$ m/s) bins

This is expected given that I_A is computed using the squared amplitudes of accelerations which can be further appreciated by observing almost doubling of the coefficient c_4 in Table 2. The median predictions are in general consistent with SA17 with differences in distance scaling of both I_A and CAV. Differences in distance scaling indicate variability in regional attenuation that is captured by the two datasets.

Figure 6 depicts comparison of median predictions from the proposed I_A and CAV models with that from SA17 models. The median predictions from this study and those from SA17 models are in general good agreement both at $R=30$ and 80 km. However, one can observe large difference in scaling at $M_w < 5.0$. We mainly attribute this to the differences in underlying datasets because the functional dependence over magnitude is identical in both the models. Moreover, it is worth mentioning that the SA17 model utilizes events with $M_w \geq 4$ whereas in the present study we consider events $M_w \geq 3$. Note that, the difference in magnitude scaling at smaller magnitudes was also observed for D_{5-75} in Fig. 4.

Furthermore, Figs. S1 and S2 depict distance ($M_w=5$) and magnitude ($R=30$ km) scaling for D_{5-75} , D_{5-95} , I_A , and CAV models.

6 Residuals

The robustness of the selected functional form (and derived coefficients) of the four models is evaluated by analysing residual trends. As an outcome of our mixed effects regression analysis (Bates et al. 2015) using Eqs. (4–7), we obtain residuals that are decomposed into event-specific between-event and within-event components. The δB_e are expected to capture source related variation (such as the stress parameter and radiation pattern) with respect to the average (median) model, while the δWS_{es} represent path specific variations in recorded ground motion along with differences in site-characteristics of the station sites. The path-specific variation for I_A and CAV represent the variations in attenuation regime while for ground-motion duration they reflect dispersion and scattering effects.

Figures 7, 8, 9 and 10 show the variations of residuals from four models for D_{5-75} , D_{5-95} , I_A and CAV, respectively. Panels (a) in Figs. 7, 8, 9 and 10 show variation of δB_e against magnitude. A rather unbiased variation of δB_e with magnitude (for all four models) suggests the sufficiency of quadratic magnitude scaling term in Eq. (5). Similarly, panels (b) in Figs. 7, 8, 9 and 10 show variation of δWS_{es} against hypocentral distance for all four models. A relatively large variability can be observed in δWS_{es} , however, there is no significant bias observed with distance except very minor overprediction (for D_{5-75} and D_{5-95}) and minor underprediction for I_A and CAV at larger distances. Panels (c) in Figs. 7, 8, 9 and 10 show variation of the station-averaged δWS_{es} (i.e., δS_{S2S}) against V_{S30} . Clearly, we do not observe any systematic trends of δS_{S2S} with V_{S30} , indicating that a linear site-response term is sufficient to capture the site-effects in the data. In general, the variability (or spread) in residuals is smallest for D_{5-95} and largest for I_A . A larger spread in I_A is expected as an effect of squared amplitudes used for its computation. However, a larger spread in D_{5-75} residuals in comparison to that for D_{5-95} is rather intriguing.

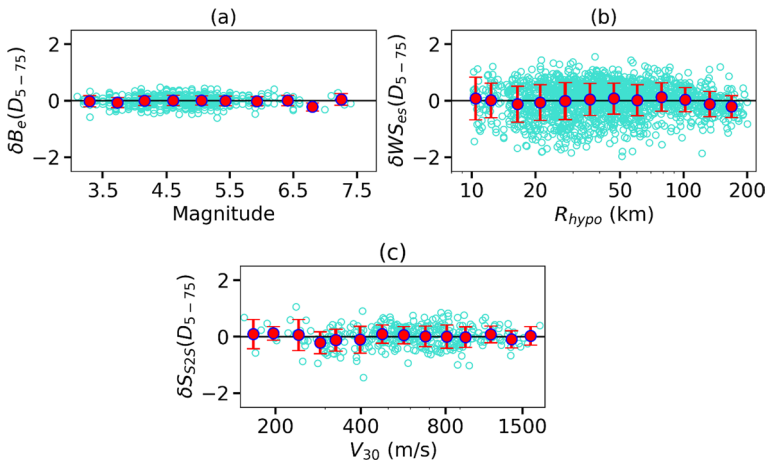


Fig. 7 **a** Between-event significant duration (5–75%) residuals (δB_e) against magnitude. The dots with vertical bars (error bars) indicate mean residuals and the standard deviation of the mean in 0.5 magnitude bins. **b** Within-event significant duration (5–75%) residuals (δWS_{es}) against hypocentral distance. The dots with vertical bars (error bars) indicate mean residuals and the standard deviation of the mean in equally spaced (in log) distance bins. **c** Averaged within-event residuals at each station (i.e., δS_{S2S}) against station V_{S30} values. The dots with vertical bars (error bars) indicate mean residuals and the standard deviation of the mean in 100 m/s V_{S30} bins

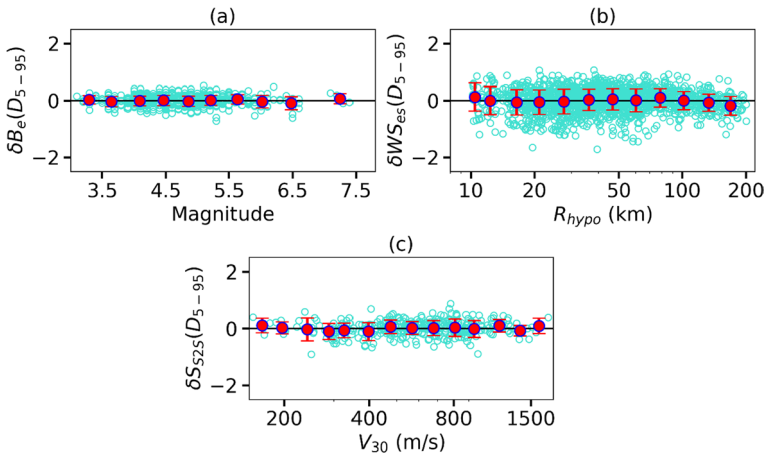


Fig. 8 **a** Between-event significant duration (5–95%) residuals (δB_e) against magnitude. The dots with vertical bars (error bars) indicate mean residuals and the standard deviation of the mean in 0.5 magnitude bins. **b** Within-event significant duration (5–95%) residuals (δWS_{es}) against hypocentral distance. The dots with vertical bars (error bars) indicate mean residuals and the standard deviation of the mean in equally spaced (in log) distance bins. **c** Averaged within-event residuals at each station (i.e., δS_{S2S}) against station V_{S30} values. The dots with vertical bars (error bars) indicate mean residuals and the standard deviation of the mean in 100 m/s V_{S30} bins

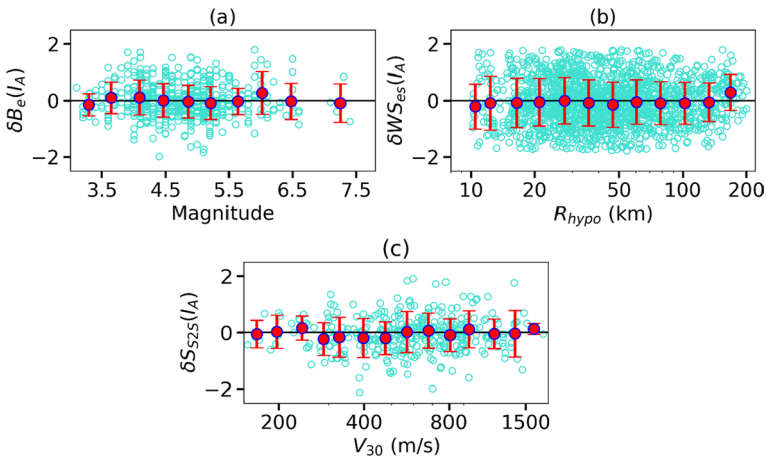


Fig. 9 **a** Between-event I_A residuals (δB_e) against magnitude. The dots with vertical bars (error bars) indicate mean residuals and the standard deviation of the mean in 0.5 magnitude bins. **b** Within-event I_A residuals (δWS_{es}) against hypocentral distance. The dots with vertical bars (error bars) indicate mean residuals and the standard deviation of the mean in equally spaced (in log) distance bins. **c** Averaged within-event residuals (i.e., δS_{S2S}) at each station against station V_{S30} values. The dots with vertical bars (error bars) indicate mean residuals and the standard deviation of the mean in 100 m/s V_{S30} bins

We also provide an estimate of aleatory variability involved in all four models for D_{5-75} , D_{5-95} , I_A and CAV. The total aleatory variability (σ) can be computed, using the following equation as a combination of τ and ϕ :

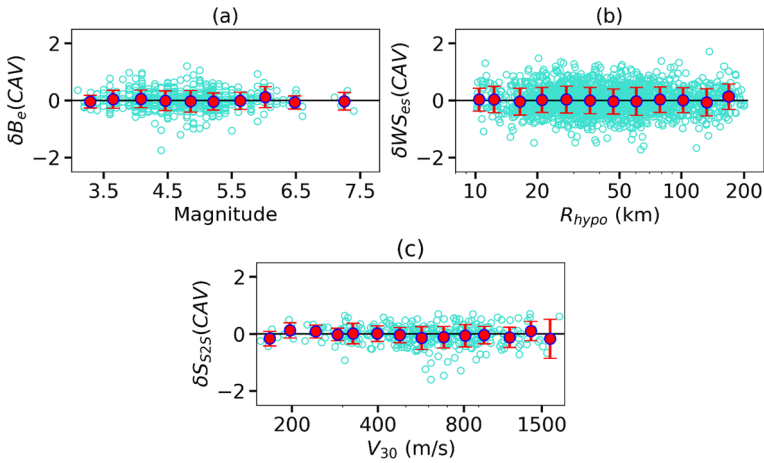


Fig. 10 **a** Between-event CAV residuals (δB_e) against magnitude. The dots with vertical bars (error bars) indicate mean residuals and the standard deviation of the mean in 0.5 magnitude bins. **b** Within-event CAV residuals (δWS_{es}) against hypocentral distance. The dots with vertical bars (error bars) indicate mean residuals and the standard deviation of the mean in equally spaced (in log) distance bins. **c** Averaged within-event residuals (i.e., δS_{S2S}) at each station against station V_{30} values. The dots with vertical bars (error bars) indicate mean residuals and the standard deviation of the mean in 100 m/s V_{30} bins

$$\sigma = \sqrt{\tau^2 + \phi^2} \tag{8}$$

The total standard deviation (σ) for significant duration (D_{5-75} and D_{5-95}) are presented in Table 1 and for I_A and CAV in Table 2. The relatively large standard deviation associated with I_A is consistent with findings of Campbell and Bozorgnia (2012, 2019), SA17 and Farhadi and Pezeshk (2020). Figure S3 shows the comparison of aleatory uncertainty for all models from this study with that from SA17 models. As noted earlier, both the τ and ϕ are largest for I_A (due to its definition) whereas τ is comparable for the two durations D_{5-75} and D_{5-95} but, ϕ is significantly larger for D_{5-75} . This indicates that D_{5-75} is rather sensitive to path and site related variations in comparison to D_{5-95} .

7 Empirical correlation analyses

In this section, we present empirical correlations between the different pairs of GMIMs used in this study. The correlation between two GMIMs can be evaluated by the correlation between the corresponding residuals of the two GMIMs (Baker and Jayaram 2008; Bradley 2015; Baker and Bradley 2017). As derived in this study and prescribed by most of the modern ground motion models (GMMs), in a mixed-effects regression algorithm, residuals are decomposed into δB_e and δWS_{es} components. Thus, in a first step, we estimate the linear correlations separately for δB_e and δWS_{es} assuming that they are independent normal variate using the following Eq. (9) (Ang and Tang 2007; Baker and Jayaram 2008; Bradley 2012):

$$\rho_{x,y} = \frac{\sum_n [(x - \bar{x})(y - \bar{y})]}{\sqrt{\sum_n [(x - \bar{x})^2] \sum_n [(y - \bar{y})^2]}} \quad (9)$$

where x and y are generic variables (i.e., in this case δB_{e_i} and δB_{e_j} for the between-event correlation and δWS_{es_i} and δWS_{es_j} for the within-event correlation), \bar{x} and \bar{y} are the sample means of x and y ; and $\sum_n []$ represents summation over the number of earthquakes (for computation of the between-event correlation), or over the number of ground motion records (for computation of the within-event correlation). Thus, this equation can be used to estimate $\rho_{\delta B_{e_i}, \delta B_{e_j}}$ (between-event correlation), $\rho_{\delta WS_{es_i}, \delta WS_{es_j}}$ (within-event correlation) and $\rho_{\epsilon_i, \epsilon_j}$ (total residuals correlation). Here i and j represent the two GMIMs considered to compute the correlation for example: $i = I_A$ and $j = D_{5-95}$. We have presented a quantile-quantile plot (Figures S4 and S5) of both the between-event (δB_{e_i}) and the within-event (δWS_{es_j}) residuals of D_{5-75} , D_{5-95} , I_A and CAV. It can be observed in both cases that the observed residual distribution is close to a normal distribution, with slight discrepancy towards the tail of the distribution. Figure S6 illustrates the distributions of the (normalized) between- and within-event residuals for the D_{5-75} , D_{5-95} , I_A , and CAV. For comparison, the (theoretical) standard normal distribution and Kolmogorov–Smirnov goodness-of-fit bounds (at the 5% significance level) are also shown. The fact that both between- and within-event distributions lie within the Kolmogorov–Smirnov goodness-of-fit bounds illustrates the applicability of the models. Also, a Kolmogorov–Smirnov test indicated that the hypothesis that the δB_{e_i} and δWS_{es_j} are normally distributed could not be rejected at the 5% significance level. Note that we compute the correlations using the standardized residuals (with zero mean and unity standard-deviation).

7.1 Uncertainty in the correlation coefficient

Usually, correlation coefficients between various GMIMs are considered stable (Baker and Bradley 2017) thus the major source of uncertainty in the point estimate of the correlation coefficient is attributed to sampling uncertainty. We quantify the sampling uncertainty in our point estimates of linear correlation using bootstrap approach (Efron 1979; Efron and Tibshirani 1993; Bradley 2012, 2015) to account for the finite number of sample sizes uncertainty. This approach uses random bootstrap samples with replacement from the observed data to calculate the correlation coefficient ρ for each bootstrap replicate. We performed 200 bootstraps and evaluated the mean and standard deviation of these 200 iterations for correlation findings to assess the stability of the results. The bootstrap means and standard deviations are summarised in Tables S5 and S7. Some earlier studies have found that the correlations between response spectral ordinates have been stable between different datasets such as NGAWest2 (Baker and Bradley 2017) and NGAWest1 (Baker and Jayaram 2008). Moreover, often the correlations (between GMIMs) are considered rather insensitive with respect to rupture scenarios as well (Baker and Jayaram 2008). However, as shown later, we have observed significant scenario dependence of the linear correlations between different GMIMs with the current dataset.

To facilitate easy comparison with other studies and for further applications, we combined the δB_{e_i} and δWS_{es_j} correlations to get the correlation between the total residuals. Using the

definition of the correlation coefficient, the correlation between the total residuals (ϵ) can then be found from the individual correlations of δB_{e_i} and δWS_{es_j} using the following equation (Bradley 2011a, 2012):

$$\rho_{\epsilon_i, \epsilon_j} = \frac{1}{\sigma_i \sigma_j} \left[\rho_{\delta B_{e_i}, \delta B_{e_j}} \tau_i \tau_j + \rho_{\delta WS_{es_i}, \delta WS_{es_j}} \phi_{ss_i} \phi_{ss_j} \right] \quad (10)$$

7.2 Correlation results

Figure 11 and Table S5 provide a summary of the Pearson correlation coefficients of the δB_e and δWS_{es} for different pairs of GMIMs. We observe in general rather low to moderate degree of correlations between I_A and the two duration measures (D_{5-75} , and D_{5-95}) for both δB_e and δWS_{es} . The negative values of correlations for both δB_e and δWS_{es} between I_A and the significant duration measures is consistent with previous studies (Bradley 2015) and the notion that a lower than average amplitude usually corresponds to a higher than average duration of ground-motion (or vice-versa) as the wave energy (power in this case) gets distributed over a longer interval of time in the seismogram. A relatively higher degree of negative correlation between I_A and D_{5-95} in comparison to I_A and D_{5-75} essentially reflects that a significant portion of energy is distributed over a longer duration in the time-histories from the current dataset. It is noteworthy that the correlations are relatively stronger (in their magnitude) for δWS_{es} in comparison to that for δB_e . The correlations between CAV and the two duration measures (D_{5-75} , and D_{5-95}) are quite small for both δB_e and δWS_{es} . However, we believe that a relatively higher (negative) correlation between I_A and the two duration measures is consistent as D_{5-75} ,

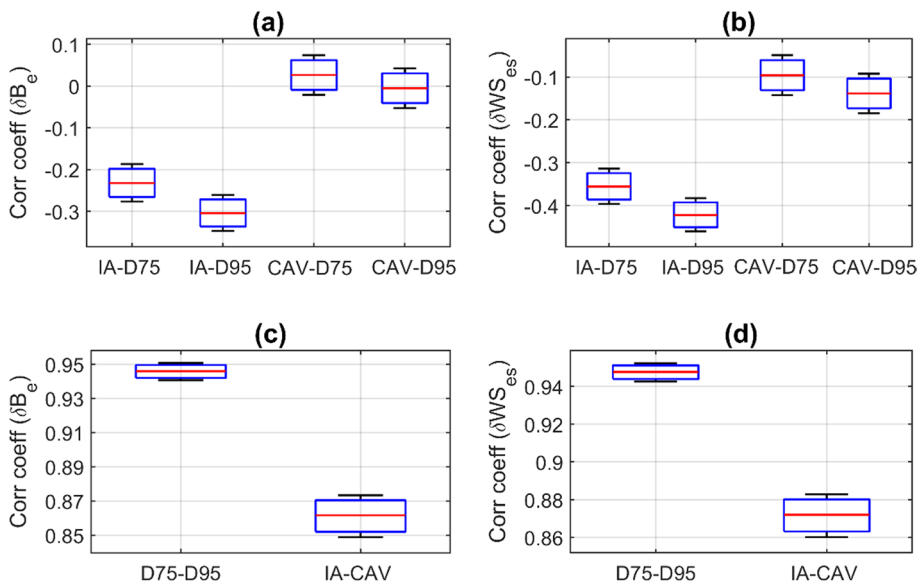


Fig. 11 Box plots of Pearson Correlation Coefficients of (a and c) the between-event (δB_e) and (b and d) within-event (δWS_{es}) residuals obtained between D_{5-75} , D_{5-95} , I_A , and CAV. On each box, the central mark (horizontal red lines) indicates the median, and the bottom and top edges of the box indicate the 25th and 75th percentiles (first and third quintile.) The black horizontal lines are minimum and maximum values

and D_{5-95} are defined based on the cumulative sum of squared acceleration amplitudes. The correlation between δB_e of CAV with I_A is 0.9459 (very high degree correlation). The correlation between δWS_{es} of CAV with I_A is 0.9476 (very high degree correlation). This shows that overall CAV and I_A are highly correlated which is unsurprising, given that they are both cumulative measures of a ground motions intensity.

We further evaluate the residual correlations in various magnitudes and distance bins as an indicative of scenario dependence of the correlations. Figures 12, 13 and 14 illustrate the observed empirical correlations of δB_e and δWS_{es} in different magnitudes, distance and V_{S30} bins respectively for various pairs of I_A , CAV, D_{5-75} and D_{5-95} . For Fig. 12, we consider simple magnitude bins M_w 3–4, M_w 4–5, M_w 5–6 and M_w 6–7 and the average correlations are plotted at the mid-points of these bins along with the bin scatter. The average correlation values may get affected by the bin-width chosen here nevertheless, they provide an average trend captured by the data. Figure 12a illustrates that the negative correlation (of δB_e) between I_A and D_{5-75} increases in amplitude as the event magnitude increases. At smaller magnitudes M_w 3–4, the correlation is close to zero whereas for the moderate magnitude range M_w 4–5, M_w 5–6 it is a moderate degree correlation with -0.2536, -0.2631 values in the respective bins. The largest correlation is ~ -0.5 observed in the M_w 6–7 bin. A similar trend is observed in Fig. 12b with slightly larger values of correlations in each bin. This is an interesting observation from the point of view that larger magnitude earthquakes

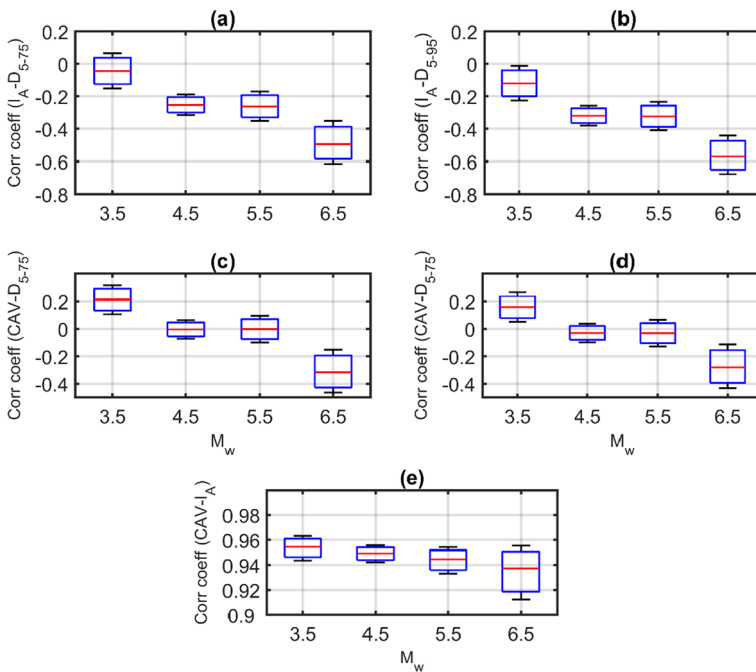


Fig. 12 Box plots of Pearson Correlation Coefficients of the between-event residuals (δB_e) obtained between: (a) I_A and D_{5-75} ; (b) I_A and D_{5-95} ; (c) CAV and D_{5-75} ; (d) CAV and D_{5-95} and (e) CAV and I_A in magnitude bins for M_w 4–5, M_w 5–6 and M_w 6–7. On each box, the central mark (horizontal red lines) indicates the median, and the bottom and top edges of the box indicate the 25th and 75th percentiles (first and third quintile) in each magnitude bin, respectively. The black horizontal lines are minimum and maximum values

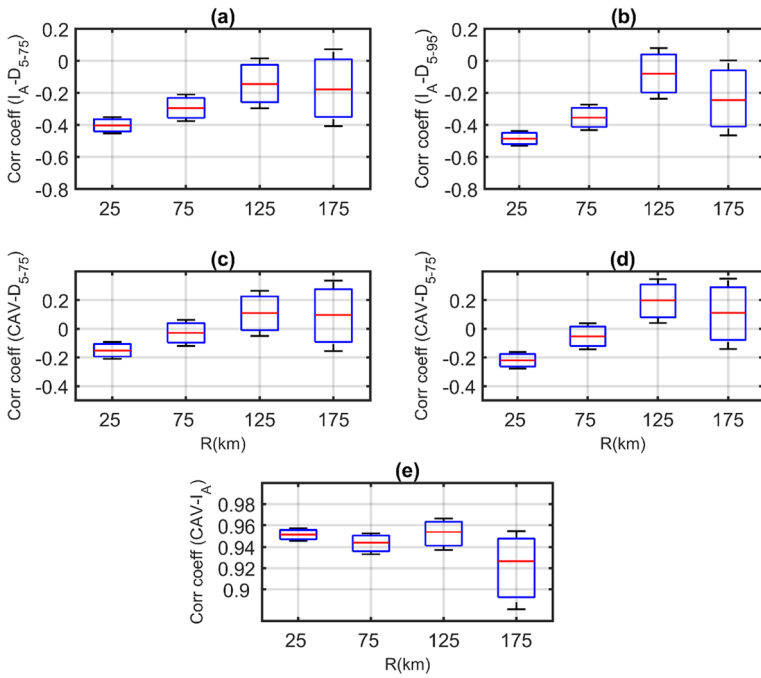


Fig. 13 Box plots of Pearson Correlation Coefficients of the within-event residuals (δWS_{es}) obtained between: (a) I_A and D_{5-75} ; (b) I_A and D_{5-95} ; (c) CAV and D_{5-75} ; (d) CAV and D_{5-95} and (e) CAV and I_A in distance bins for R_{hypo} 10–50, R_{hypo} 50–100, R_{hypo} 100–150 and R_{hypo} 150–200 km. On each box, the central mark (horizontal red lines) indicates the median, and the bottom and top edges of the box indicate the 25th and 75th percentiles (first and third quintile) in each R_{hypo} bin, respectively. The black horizontal lines are minimum and maximum values

produce more low-frequency energy as the corner frequency of the event gets smaller with the increase in event magnitude. We are aware that these correlations are affected by the standard-deviation of the residuals as well (see Eq. 9). Hence, we plotted the τ in same magnitude bins (M_w 3–4, M_w 4–5, M_w 5–6 and M_w 6–7) for all the GMIMs as given in supplementary Figure S7. We can appreciate that the low degree of correlation in M_w 3–4 and M_w 4–5 bins is explained by relatively larger standard-deviation (τ in this case) but for M_w 5–6 and M_w 6–7 it does not fully explain the observed trend in Figs. 12a and b. Figures 12c and d show the correlations (of δB_e) between CAV- D_{5-75} and CAV- D_{5-95} , respectively. A similar trend is observed in this case, for M_w 3–4 the correlations are positive with low degree of correlations (~ 0.2 and ~ 0.15). In the moderate magnitude range M_w 4–5, M_w 5–6, the correlations are close to zero (-0.0016 , -0.0294) whereas in the larger magnitude range M_w 6–7 there is comparatively stronger negative correlations (-0.3167 , -0.2803). A slightly stronger negative correlation for M_w 6–7 seems consistent with the notion that CAV captures low-to-moderate frequency range of ground motion. Figure 12e shows the correlation (of δB_e) between I_A and CAV. In this case, the (positive and high degree) correlation values are relatively stable across different magnitude bins with lowest for M_w 6–7 range. This again suggests that I_A and CAV may capture slightly different frequency ranges that are present in the ground-motion.

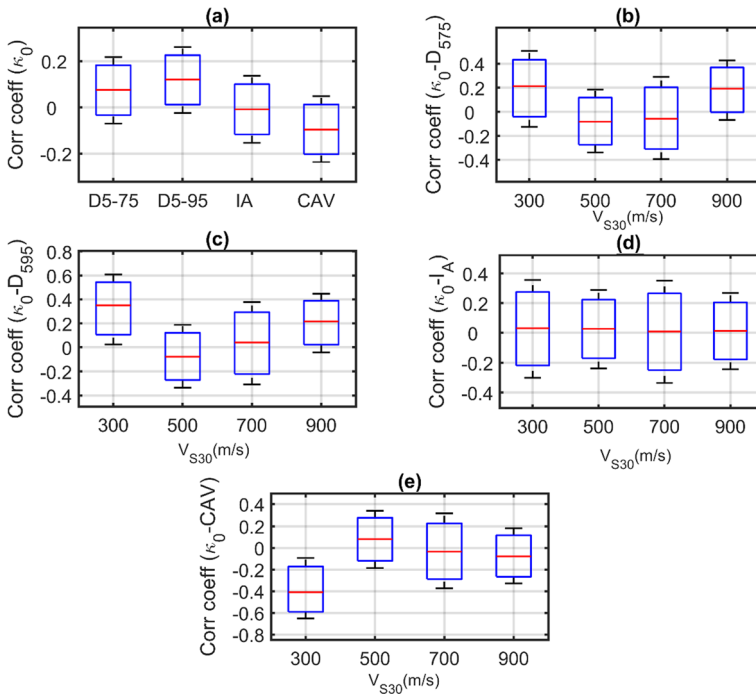


Fig. 14 **a** Box plots of Pearson Correlation Coefficients of the within-event residuals (δWS_{es}) obtained between D_{5-75} , D_{5-95} , I_A and CAV with κ_0 . On each box, the central mark (horizontal red lines) indicates the median, and the bottom and top edges of the box indicate the 25th and 75th percentiles (first and third quintile) respectively. **b**, **c**, **d** and **e** Box plots of Pearson Correlation Coefficients of the within-event residuals (δWS_{es}) obtained between D_{5-75} , D_{5-95} , I_A and CAV with κ_0 in V_{S30} bins for V_{S30} 200–400, V_{S30} 400–600, V_{S30} 600–800 (m/s) and $800 < V_{S30}$ (m/s). On each box, the central mark (horizontal red lines) indicates the median, and the bottom and top edges of the box indicate the 25th and 75th percentiles (first and third quintile) in each V_{S30} bin, respectively. The black horizontal lines are minimum and maximum values

Figure 13 shows the correlation of δWS_{es} in four different distance bins for different pairs of GMIMs as considered in Fig. 12. For Fig. 13, we consider four broad distance bins with R_{hypo} 10–50 km, 50–100 km, 100–150 km and 150–200 km. Average correlations along with the bin spreads (25th and 75th percentiles) are plotted at the mid-point of these bins. We have considered rather broad bins to capture more observations hence to get a stable estimate of average values. Figures 13a and b show the correlations for I_A - D_{5-75} and I_A - D_{5-95} , respectively. Except the differences in absolute values of the correlations the trend of decreasing correlation with increasing distance is similar in both the figures. The strongest negative correlation between I_A and the two duration measures is found to be in the near distance ranges ($R_{hypo} < 100$ km). Beyond $R_{hypo} > 100$ km the correlation between the pair of GMIMs is negligible. This observation is again consistent with the seismological theory that with increasing distance there are more scattered wave arrivals which often form the coda part of the seismogram. In the near distance range ($R_{hypo} < 50$ –70 km) most of the energy in the seismogram is due to the direct S-wave arrivals. Supplementary Figure S8 shows values of ϕ in the same distance bins for all four GMIMs. The ϕ values are lowest (relative to other bins for all the four GMIMs) in the distance range $R_{hypo} > 100$ km hence they do not account for the low values of correlation in these distance ranges. Figure 13e

shows the correlations (of δWS_{es}) between CAV and I_A in the distance bins considered here. The correlations are rather stable with respect to distance with slightly lower values and larger scatter in the distance bin R_{hypo} 150–200 km.

We further investigated the correlation of δWS_{es} (for D_{5-75} , D_{5-95} , I_A , and CAV) with κ_0 (near-surface attenuation parameter) (Table S6) at each station. Out of 338 stations, κ_0 was available for 215 stations from the study of Davatgari-Tafreshi et al. (2022). Figure 14a illustrates the correlations for D_{5-75} , D_{5-95} , I_A , and CAV together in a single plot. In general, the values of the correlations are very low between κ_0 and the GMIMs considered here. However, the sign of correlation is positive between κ_0 and the two SD measures. Interestingly, the correlation between δWS_{es} (for I_A) and κ_0 is quite close to zero. This observation is contrary to the popular notion that I_A as the representative of high-frequency ground motions. In fact, the correlation between δWS_{es} (for CAV) and κ_0 has negative sign which is consistent with how CAV is defined. We further explore these correlations by plotting them in different V_{S30} bins. For that purpose, we consider four V_{S30} bins: V_{S30} 200–400, V_{S30} 400–600, V_{S30} 600–800 (m/s) and $V_{S30} > 800$ m/s. Average correlations (along with associated scatter) are plotted at the mid-point of these bins. Clearly, there is a V_{S30} dependence of the correlations between δWS_{es} and the two duration measures (D_{5-75} and D_{5-95}) with a slight (positive) correlations in V_{S30} : 200–400 m/s. The correlation between δWS_{es} (for I_A) and κ_0 does not show any V_{S30} dependence. On the other hand, a moderate degree of negative correlation (~ -0.4) between δWS_{es} (for CAV) and κ_0 is observed in V_{S30} bin: 200–400 m/s. At other V_{S30} values this correlation is negligibly small close to zero.

Table S7 and Figure S9 summarise the Pearson Correlation Coefficients of the total residuals, computed using Eq. (10), in this study. Our results show that D_{5-75} and D_{5-95} have a high degree correlation (0.8613). This is consistent with Bradley's (Bradley 2011b) results (0.843). An imperfect correlation between D_{5-75} and D_{5-95} essentially suggests how these two measures of duration capture different information from the acceleration time-histories. In our study, total residual of I_A negatively correlates (moderate degree correlation) with D_{5-75} (-0.3240) and D_{5-95} (-0.3932). Bradley (2015) observed that I_A negatively correlates with D_{5-75} (-0.19) and D_{5-95} (-0.20). The results of the two studies are not identical, but they are comparable. The total residual-correlation between CAV and the two duration measures is very low: D_{5-75} (-0.0699), and D_{5-95} (-0.1028). Bradley (2011b) also observed that CAV has a very small positive correlation with D_{5-75} (0.08) and D_{5-95} (0.12). At first the relatively small correlation of CAV with significant duration measures may appear contrary to the notion that CAV carries more information regarding duration than the I_A (Campbell and Bozorgnia 2010; Macedo et al. 2020). The lack of correlation between CAV and significant duration can be understood through Fig. 14 in which we observed a negative correlation between CAV and κ_0 whereas, D_{5-75} and D_{5-95} are weakly (but positive) correlated with κ_0 . Thus, one can appreciate the weak negative correlation between CAV and the two duration measures as an outcome of the two competing effects at play here. It is widely accepted that parameter κ_0 reflects high-frequency behaviour (Anderson and Hough 1984) of ground-motion in Fourier domain. A relatively strong (negative) correlation between CAV and κ_0 in comparison to that between I_A and κ_0 indicates that CAV is more representative of high-frequency ground motion. The often observed high correlation of I_A with PSA (spectral pseudo-acceleration) at shorter periods (Bradley 2012, 2015) can be understood by observing similarity between the definition of I_A (Eq. 1) and the zeroth spectral moment of the single degree of freedom (SDOF) oscillator response (Bora et al. 2016; Eqs. (19) and (20) in Kolli and Bora 2021) through Parseval's theorem. Thus, similar to PGA (and other short period PSAs), I_A is affected by a broad range of frequencies in the ground-motion not just the high frequencies. This can be

partially appreciated by observing a stronger negative correlation (of δB_e) between I_A and D_{5-75} , D_{5-95} for larger magnitudes in Fig. 12. Events with larger magnitude are rich in low-frequency content.

We have observed strong positive correlation (very high degree correlation) between I_A and CAV (0.9435) as also observed by Bradley (2015) (0.89) and Campbell and Bozorgnia (2012) (0.923). Farhadi and Pezeshk (2020) mentioned that the Pearson correlation coefficients equal 0.959, suggesting a very high correlation between I_A and CAV. An imperfect correlation between I_A and CAV clearly suggests that they are sensitive to different frequency ranges in the ground-motion as has been discussed here.

8 Conclusions

In this study, we derive empirical models for four GMIMs namely, I_A , CAV, D_{5-75} , and D_{5-95} . A common functional form was used to model the observed scaling of the selected GMIMs over magnitude, distance and V_{S30} to facilitate easy comparison and interpretation of the derived coefficients (model parameters). The models are calibrated on 1749 acceleration (horizontal) time histories compiled by the Building and Housing Research Center (BHRC) of Iran originated from 566 events (M_w 3–7.5) and recorded at 338 stations at $R_{\text{hypo}} \leq 200$ km in the time period from 1976 to 2020. An orientation independent measure of the ground-motion (RotD50) was used for all the GMIMs. Mixed-effects regression algorithm was employed to estimate the model coefficients and the components of uncertainty (residuals). Median predictions of I_A , CAV, D_{5-75} , and D_{5-95} were found consistent with other previously published regional and global studies with obvious differences arising from the choice of datasets and adopted functional forms. Robustness of the derived models (and coefficients) was further assessed by examining residual distributions and their variation against predictor variables such as magnitude, distance and V_{S30} . Based on residual variations and comparison with other global models, we consider these models to be valid for shallow crustal earthquakes in active tectonic regions with magnitudes (M_w) ranging from 4.0 to 7.0, and distances ranging from 20 up to 200 km.

We examined the residual correlation between different pairs of GMIMs. Overall, low-to-moderate degree of (total) correlation was found between I_A and the two SD measures. Almost no correlation was observed between CAV and the two SD measures with values -0.072 and -0.11 between CAV- D_{5-75} and CAV- D_{5-95} , respectively. As expected, a very high degree of correlation was observed between I_A and CAV however an imperfect correlation (~ 0.95) indicates that both the cumulative GMIMs capture different aspects of ground-motion. Similarly, a high degree of correlation (~ 0.87) between D_{5-75} and D_{5-95} is an indicative of their definition and how they are computed. Again, an imperfect correlation between the two SD measures clearly suggests that they may not essentially capture the same information from a ground-motion trace. The correlations were analyzed for δB_e and δWS_{es} separately which were subsequently combined to obtain correlation of total residuals. In general, the correlation values (in terms of their absolute values) are lower for δB_e in comparison to that for δWS_{es} . The uncertainty in correlation estimates was evaluated by using bootstrapping procedure.

We further investigated rupture scenario dependence of the residual correlations (for both δB_e and δWS_{es}) in different magnitudes and distance bins. The negative correlations of δB_e between I_A and the two SD measures were found strongest for larger magnitude

events $M_w > 6$. Almost no correlation was found for $M_w < 4.0$ between the two GMIMs whereas in the moderate magnitude range M_w 4–6 the correlation was rather low. A similar trend was observed for the correlations of δB_c between CAV and the two SD measures. Similarly, the correlations for δWS_{es} between I_A and the two SD measures were found to be depending upon the distances. For both I_A - D_{5-75} and I_A - D_{5-95} the values of negative (δWS_{es}) correlations were strongest in the near distance range $R_{\text{hypo}} < 50$ km with values decreasing with increase in distance. Almost no correlation ($< \sim 0.2$) was observed beyond 100 km distance. A similar trend (with slightly lower values) was observed for the correlations of δWS_{es} between CAV and the two SD measures.

We further investigated the correlations of δWS_{es} (for all four GMIMs) with station-specific κ_0 values. In general, the values of the correlations (correlation of δWS_{es}) are very low between κ_0 and the GMIMs considered here. We observed positive correlation between κ_0 and the two SD measures, and correlation value quite close to zero between I_A (correlation of δWS_{es}) and κ_0 . A relatively stronger negative correlation was observed between CAV and κ_0 in comparison to that between I_A – κ_0 . A close-to-zero correlation between I_A and κ_0 is opposite to the popular notion of I_A being more representative of high-frequency ground-motions in comparison to CAV. At sites with lower V_{S30} values, the negative correlation (-0.4) between CAV and κ_0 was evident. The relatively strong (negative) correlation between δWS_{es} (for CAV) and κ_0 is consistent with how CAV is defined.

Correlation models (e.g., Bradley 2012a, b) between different GMIMs are key components in the application of vector probabilistic seismic hazard analysis (VPSHA) and the generalized conditional intensity measure (GCIM) methods (Bazzurro 1998; Baker and Cornell 2005; Bradley 2012). In this context, clearly, the results particularly with regard to residual correlations represent the seismological characteristics and properties captured by the current dataset. Nevertheless, the analysis in this article presents significant new insights with regard to residual correlations (between GMIMs considered here) and their scenario dependence which has broader implications for engineering applications such as VPSHA and ground-motion selection. Clearly, a thorough investigation of residual correlations (between various GMIMs) is warranted for other geographical regions as well with much larger datasets which cover broader event magnitude range than that is covered by the current dataset.

9 Data and resources

The data underlying this article were accessed from the Building and Housing Research Center (BHRC) of Iran (<http://www.bhrc.ac.ir/>, last accessed December 2020). The derived data generated in this research will be shared on reasonable request to the corresponding author. The supplemental material to this article includes nine figures, which provides comparisons of distance and magnitude scaling for the significant duration (D_{5-75} and D_{5-95}), I_A and CAV models, variations in between-event, within event and total standard deviation for models, the quantile-quantile plot of the between-event and within-event residuals, distributions of normalized between-event; and normalized within-event residuals, box plots of between-event standard deviation (τ) and within-event standard deviation (ϕ), and box plots of Pearson Correlation Coefficients of the total residuals, and seven tables, which contain, coefficients covariance, the summary of the Pearson Correlation Coefficients of the

between-event and within-event residuals, the Pearson Correlation Coefficients of within-event residuals with κ_0 , and the Pearson Correlation Coefficients of the total residuals.

Supplementary Information The online version contains supplementary material available at <https://doi.org/10.1007/s10518-023-01708-9>.

Acknowledgements The authors thank the Building and Housing Research Center of Iran for generously providing the data for this work. The authors thank Associate Editor John Douglas and two anonymous reviewers for their constructive reviews on this article.

Funding The authors declare that no funds and grants were received during the preparation of this manuscript.

Declarations

Conflict of interest The authors acknowledge that there are no conflicts of interest recorded.

References

- Abrahamson C, Shi H-JM, Yang B (2016) Ground-motion prediction equations for Arias intensity consistent with the NGA-West2 ground-motion models, PEER report 2016/ 05. University of California, Pacific Earthquake Engineering Research Center, Berkeley
- Afshari K, Stewart JP (2016) Physically parameterized prediction equations for significant duration in active crustal regions. *Earthq Spect* 32(4):2057–2081
- Akkar S, Sandikkaya MA, Ay BO (2014) Predictive models for horizontal and vertical conditional mean response spectra at multiple damping levels derived for Europe and the Middle East. *Bull Earthq Eng* 12:517–547
- Al Atik L, Abrahamson N, Bommer JJ, Scherbaum F, Cotton F, Kuehn N (2010) The variability of ground-motion prediction models and its components. *Seismol Res Lett* 81(5):794–801
- Ancheta TD, Darragh RB, Stewart JP, Seyhan E, Silva WJ, Chiou BS-J, Wooddell KE, Kottke AR, Boore DM, Kishida T, Donahue JL (2014) NGA-west2 database. *Earthq Spect* 30:989–1005
- Ang AHS, Tang WH (2007) Probability concepts in engineering: emphasis on applications in civil and environmental engineering. Wiley, New York
- Anderson JG, Hough SE (1984) A model for the shape of the Fourier amplitude spectrum of acceleration at high frequencies. *Bull Seism Soc Am* 74(5):1969–1993. <https://doi.org/10.1785/BSSA0740051969>
- Arias A (1970) A measure of earthquake intensity. In: Hansen R (ed) *Seismic design for nuclear power plants*. MIT Press, Cambridge, pp 438–483
- Azizi K, Kashani AR, Ebrahimi S, Jazaei F (2022) Application of a multi-objective optimization model for the design of piano key weirs with a fixed dam height. *Can J Civ Eng* 49(11):1764–1778
- Bahrampouri M, Rodriguez-Marek A, Green RA (2020) Ground motion prediction equations for significant duration using the kik-net database. *Earthq Spect* 37:903
- Baker JW, Cornell CA (2005) A vector-valued ground motion intensity measure consisting of spectral acceleration and eplison. *Earthq Eng Struct Dyn* 34(10):1193–217
- Baker JW (2007) Probabilistic structural response assessment using vector-valued intensity measures. *Earthq Eng Struct Dyn* 36(13):1861–1883. <https://doi.org/10.1002/eqe.700>
- Baker JW, Jayaram N (2008) Correlation of spectral acceleration values from NGA ground motion models. *Earthq Spectra* 24(1):299–317
- Baker JW, Bradley BA (2017) Intensity measure correlations observed in the NGA-West2 database, and dependence of correlations on rupture and site parameters. *Earthq Spectra* 33(1):145–156
- Bates D, Mächler M, Bolker BM, Walker SC (2015) Fitting linear mixed-effects models using lme4. *J Stat Softw* 67(1):1–48
- Bazzurro P (1998) Probabilistic seismic demand analysis. Palo Alto, Stanford University, CA, p 329
- Bommer JJ, Martínez-Pereira A (1999) The effective duration of earthquake strong motion. *J Earthquake Eng* 3(2):127–172
- Bommer JJ, Magenes G, Hancock J, Penazzo P (2004) The influence of strong-motion duration on the seismic response of masonry structures. *Bull Earthq Eng* 2(1):1–26

- Bommer JJ, Stafford PJ, Alarcón JA (2009) Empirical equations for the prediction of the significant, bracketed, and uniform duration of earthquake ground motion. *Bull Seism Soc Am* 99(6):3217–3233
- Boore DM (2003) Simulation of ground motion using the stochastic method. *Pure Appl Geophys* 160(3):635–676. <https://doi.org/10.1007/PL00012553>
- Boore DM, Akkar S (2003) Effect of causal and acausal filters on elastic and inelastic response spectra. *Earthq Eng Struct Dyn* 32:1729–1748
- Boore DM (2005) SMSIM—Fortran programs for simulating ground motions from earthquakes: version 2.3—a revision of OFR 96–80–A, available at: <http://www.daveboore.com/smsim> (last accessed October 2021).
- Boore DM, Bommer JJ (2005) Processing of strong-motion accelerograms: needs, options and consequences. *Soil Dyn Earthq Eng* 25:93–115
- Boore DM (2010) Orientation-independent, nongeometric-mean measures of seismic intensity from two horizontal components of motion. *Bull Seism Soc Am* 100:1830–1835
- Boore DM, Thompson EM (2014) Path durations for use in the stochastic-method simulation of ground motions. *Bull Seism Soc Am* 104:2541–2552
- Bora SS, Scherbaum F, Kuehn N, Stafford P (2014) Fourier spectral- and duration models for the generation of response spectra adjustable to different source-, propagation-, and site conditions. *Bull Earthq Eng* 12(1):467–493
- Bora SS, Scherbaum F, Kuehn N, Stafford P, Edwards B (2015) Development of a response spectral ground-motion prediction equation (GMPE) for seismic-hazard analysis from empirical Fourier spectral and duration models. *Bull Seism Soc Am* 105:2192–2218
- Bora SS, Cotton F, Scherbaum F (2019) NGA-West2 empirical Fourier and duration models to 7 generate adjustable response spectra. *Earthq Spectra* 35:61–93. <https://doi.org/10.1193/110317eqs228m>
- Bradley BA, Cubrinovski M, Dhakal RP, MacRae GA (2009) Intensity measures for the seismic response of pile foundations. *Soil Dyn Earthq Eng* 29:1046–1058
- Bradley BA (2010) A generalized conditional intensity measure approach and holistic ground-motion selection. *Earthq Eng Struct Dynam* 39(12):1321–1342
- Bradley BA (2011a) Empirical correlation of PGA, spectral accelerations and spectrum intensities from active shallow crustal earthquakes. *Earthq Eng Struct Dynam* 40(15):1707–1721
- Bradley BA (2011b) Correlation of significant duration with amplitude and cumulative intensity measures and its use in ground motion selection. *J Earthquake Eng* 15:809–832
- Bradley BA (2012) Empirical correlations between peak ground velocity and spectrum-based intensity measures. *Earthq Spectra* 28:17–35
- Bradley BA (2015) Correlation of arias intensity with amplitude, duration and cumulative intensity measures. *Soil Dynam Earthq Eng* 78:89–98
- Bray JD, Macedo J (2017) 6th Ishihara lecture: simplified procedure for estimating liquefaction-induced building settlement. *Soil Dynam Earthq Eng* 102:215–231
- Brune JN (1970) Tectonic stress and the spectra of seismic shear waves from earthquakes. *J Geophys Res* 75(26):4997–5009. <https://doi.org/10.1029/JB075i026p04997>
- Brune JN (1971) Correction. *J Geophys Res* 76(20):5002. <https://doi.org/10.1029/JB076i020p05002>
- Bullock Z, Dashti S, Karimi Z, Liel A, Porter K, Franke K (2019a) Probabilistic models for residual and peak transient tilt of mat-founded structures on liquefiable soils. *J Geotech Geoenviron Eng* 145(2):04018108. [https://doi.org/10.1061/\(ASCE\)GT.1943-5606.0002002](https://doi.org/10.1061/(ASCE)GT.1943-5606.0002002)
- Bullock Z, Dashti S, Liel AB, Porter KA, Karimi Z (2019b) Assessment supporting the use of outcropping rock, evolutionary intensity measures for prediction of liquefaction consequences. *Earthq Spectra* 35(4):1899–1926. <https://doi.org/10.1193/041618eqs094m>
- Bustos AG, and Stafford PJ (2012) On the use of Arias intensity as a lower bound in the hazard integration process of a PSHA, Proceeding. 15th World Conference on Earthquake Engineering, Vol. 12, Lisbon, Portugal, 24–28 September 2012, pp 9011–9020.
- Cabañas L, Benito B, Herraiz M (1997) An approach to the measurement of the potential structural damage of earthquake ground motions. *Earthq Eng Struct Dyn* 26:79–92
- Campbell KW, Bozorgnia Y (2010) A groundmotion prediction equation for the horizontal component of cumulative absolute velocity (CAV) based on the PEER-NGA strong motion database. *Earthq Spectra* 26(3):635–650. <https://doi.org/10.1193/1.3457158>
- Campbell KW, Bozorgnia Y (2012) A comparison of ground motion prediction equations for Arias intensity and cumulative absolute velocity developed using a consistent database and functional form. *Earthq Spectra* 28(3):931–941. <https://doi.org/10.1193/1.4000067>
- Campbell KW, Bozorgnia Y (2019) Ground motion models for the horizontal components of Arias Intensity (AI) and cumulative absolute velocity (CAV) using the NGA-west2 database. *Earthq Spectra* 35(3):1289–1310. <https://doi.org/10.1193/090818eqs212m>

- Chai YH, Fajfar P, Romstad KM (1998) Formulation of duration-dependent inelastic seismic design spectrum. *J Struct Eng* 124(8):913–921
- Chandramohan R, Baker JW, Deierlein GG (2016) Quantifying the influence of ground motion duration on structural collapse capacity using spectrally equivalent records. *Earthq Spectra* 32(2):927–950
- Cheng Y, Ning CL, Du WQ (2020) Spatial cross-correlation models for absolute and relative spectral input energy parameters based on geostatistical tools. *Bull Seism Soc Am* 110(6):2728–2742
- Cheng Y, Liu T, Wang J, Ning CL (2022) Empirical correlations of spectral input energy with peak amplitude, cumulative, and duration intensity measures. *Bull Seism Soc Am* 112(2):978–991
- Cimellaro GP (2013) Correlation in spectral accelerations for earthquakes in Europe. *Earthq Eng Struct Dynam* 42(4):623–633
- Danciu L, Tselentis G (2007) Engineering ground-motion parameters attenuation relationships for Greece. *Bull Seism Soc Am* 97(1B):162–183. <https://doi.org/10.1785/0120050087>
- Darzi A, Zolfaghari MR, Cauzzi C, Fäh D (2019) An empirical ground-motion model for horizontal PGV, PGA, and 5% damped elastic response spectra (0.01–10s) in Iran an empirical ground-motion model. *Bull. Seism. Soc. Am.* 109(3):1041–1057
- Davatgari Tafreshi M, Bora SS, Mirzaei N, Ghofrani H, Kazemian J (2021) Spectral models for seismological source parameters, path attenuation and site-effects in Alborz region of northern Iran. *Geophys J Int* 227(1):350–367. <https://doi.org/10.1093/gji/ggab227>
- Davatgari Tafreshi M, Bora SS, Ghofrani H, Mirzaei N, Kazemian J (2022) Region-and site-specific measurements of kappa (κ_0) and associated variabilities for Iran. *Bull Seism Soc Am* 112(6):3046–3062
- Douglas J (2012) Consistency of ground-motion predictions from the past four decades: peak ground velocity and displacement, Arias intensity and relative significant duration. *Bull Earthq Eng* 10:1339–1356
- Du W, Wang G (2012) A simple ground-motion prediction model for cumulative absolute velocity and model validation. *Earth Eng Struct Dynam* 42(8):1189–1202. <https://doi.org/10.1002/eqe.2266>
- Du W, Wang G (2013) A simple ground-motion prediction model for cumulative absolute velocity and model validation. *Earthq Eng Struct Dynam* 42(8):1189–1202
- Du W, Wang G (2017) Prediction equations for ground-motion significant durations using the NGA-West2 database. *Bull Seism Soc Am* 107(1):319–333
- Du W (2019) Empirical correlations of frequency-content parameters of ground motions with other intensity measures. *J Earthq Eng* 23(7):1073–1091
- Du W, Long S, Ning CL (2020) An algorithm for selecting spatially correlated ground motions at multiple sites under scenario earthquakes. *J Earthq Eng*. <https://doi.org/10.1080/13632469.2019.1688736>
- Electrical Power Research Institute (EPRI) 1988 A criterion for determining exceedance of the operating basis earthquake, EPRI NP-5930, Palo Alto, California.
- Efron B (1979) Computers and the theory of statistics: thinking the unthinkable. *SIAM Rev* 21(4):460–480
- Eferon B, Tibshirani RJ (1993) An introduction to the bootstrap. Chapman & Hall, New York
- Fahjan YM, Alcik H, Sari A (2011) Applications of cumulative absolute velocity to urban earthquake early warning systems. *J Seismol* 15(2):355–373. <https://doi.org/10.1007/s10950-011-9229-8>
- Farajpour Z, Zare M, Pezeshk S, Ansari A, Farzanegan E (2018) Nearsourc strong motion database catalog for Iran. *Arab J Geosc* 11:80
- Farhadi A, Pezeshk S (2020) A referenced empirical ground-motion model for arias intensity and cumulative absolute velocity based on the NGA-east database a referenced empirical ground-motion model for Arias intensity and cumulative absolute velocity based on the NGA-east database. *Bull Seism Soc Am* 110(2):508–518
- Foulser-Piggott R, Stafford PJ (2012) A predictive model for Arias intensity at multiple sites and consideration of spatial correlations. *Earthq Eng Struct Dyn* 41:431–451
- Foulser-Piggott R, Goda K (2015) Ground-motion prediction models for Arias Intensity and cumulative absolute velocity for Japanese earthquakes considering single-station sigma and within-event spatial correlation. *Bull Seism Soc Am* 105(4):1903–1908. <https://doi.org/10.1785/0120140316>
- Goda K (2011) Interevent variability of spatial correlation of peak ground motions and response spectra. *Bull Seism Soc Am* 101(5):2522–2531
- Hancock J, Bommer JJ (2006) A state-of-knowledge review of the influence of strong-motion duration on structural damage. *Earthq Spectra* 22(3):827–845
- Harp E, Wilson R (1995) Shaking intensity thresholds for rock falls and slides: Evidence from 1987 Whittier Narrows and Superstition Hills earthquake strong motion records. *Bull Seism Soc Am* 85(6):1739–1757
- Hou H, Qu B (2015) Duration effect of spectrally matched ground motions on seismic demands of elastic perfectly plastic SDOFS. *Eng Struct* 90:48–60
- Huang Z-K, Zhang D-M (2021) Scalar- and vector-valued vulnerability analysis of shallow circular tunnel in soft soil. *Transp Geotech* 27:100505
- Iervolino I, Manfredi G, Cosenza E (2006) Ground motion duration effects on nonlinear seismic response. *Earthq Eng Struct Dynam* 35(1):21–38

- Jaimes MA, Reinoso E, Ordaz M (2006) Comparison of methods to predict response spectra at instrumented sites given the magnitude and distance of an earthquake. *J Earthquake Eng* 10(06):887–902
- Kashani AR, Camp CV, Akhiani M, Ebrahimi S (2022) Optimum design of combined footings using swarm intelligence-based algorithms. *Adv Eng Softw* 169:103140
- Keefer DK (2002) Investigating landslides caused by earthquakes—A historical review. *Surv Geophys* 23:473–510
- Kempton JJ, Stewart JP (2006) Prediction equations for significant duration of earthquake ground motions considering site and near-source effects. *Earthq Spectra* 22(4):985–1013
- Kolli MK, Bora SS (2021) On the use of duration in random vibration theory (RVT) based ground motion prediction: a comparative study. *Bull Earthq Eng* 19(4):1687–1707
- Kramer SL, Mitchell RA (2006) Ground motion intensity measures for liquefaction hazard evaluation. *Earthq Spectra* 22(2):413–438. <https://doi.org/10.1193/1.2194970>
- Krawinkler H, Zohrei M, Lashkari-Irvani B, Cofie N, and Hadidi-Tamjed H (1983) Recommendations for experimental studies on the seismic behaviour of steel components and materials. John A. Blume Center, Report No. 61.
- Lee C-T, Hsieh B-S, Sung C-H, Lin P-S (2012) Regional Arias intensity attenuation relationship for Taiwan considering VS30. *Bull Seismol Soc Am* 102:129–142
- Lee J, Green RA (2014) An empirical significant duration relationship for stable continental regions. *Bull Earthq Eng* 12(1):217–235
- Luco N, Cornell CA (2007) Structure-specific scalar intensity measures for near-source and ordinary earthquake ground motions. *Earthq Spectra* 23(2):357–392
- Macedo, J. L. 2017. Simplified procedures for estimating Earthquake-induced displacements, Ph.D. Thesis, University of California, Berkeley.
- Macedo J, Abrahamson N, Bray JD (2019) Arias intensity conditional scaling ground-motion models for subduction zones. *Bull Seism Soc Am* 109(4):1343–1357. <https://doi.org/10.1785/0120180297>
- Macedo J, Abrahamson N, Liu C (2020) New Scenario-Based Cumulative Absolute Velocity Models for Shallow Crustal Tectonic Settings. *Bull Seism Soc Am* 111(1):1–16. <https://doi.org/10.1785/0120190321>
- Meimandi-Parizi A, Daryoushi M, Mahdavian A, Saffari H (2020) Ground-motion models for the prediction of significant duration using strong-motion data from Iran. *Bull Seism Soc Am* 110(1):319–330. <https://doi.org/10.1785/0120190109>
- Mousavi-Bafrouei SH, Babaie Mahani A (2020) A comprehensive earthquake catalogue for the Iranian Plateau (400 B.C. to December 31, 2018). *J Seismol* 24:709–724
- Muin S, Mosalam KM (2017) Cumulative absolute velocity as a local damage indicator of instrumented structures. *Earthq Spectra* 33(2):641–664. <https://doi.org/10.1193/090416EQS142M>
- Rauch AF, Martin JR III (2000) EPOLLS model for predicting average displacements on lateral spreads. *J Geotech Geoenviron Eng* 126(4):360–371
- Reinoso E, Ordaz M, Sanchez-Sesma FJ (1990) A note on the fast computation of response spectra estimates. *Earthquake Eng Struct Dynam* 19(7):971–976
- Ruiz-García J (2010) On the influence of strong-ground motion duration on residual displacement demands. *Earthq Struct.* 1:327–344
- Sandikkaya MA, Akkar S (2017) Cumulative absolute velocity, Arias intensity and significant duration predictive models from a pan-European strong-motion dataset. *Bull Earthq Eng* 15(5):1881–1898
- Sedaghati F, Pezeshk S (2017) Partially nonergodic empirical ground motion models for predicting horizontal and vertical PGV, PGA, and 5% damped linear acceleration response spectra using data from Iranian plateau. *Bull Seismol Soc Am* 107:934–948
- Seed HB, Idriss IM (1982). Ground motions and soil liquefaction during earthquakes. Earthquake engineering research institute, Oakland California, pp 1–12
- Shome N, Cornell CA, Bazzurro P, Carballo JE (1998) Earthquakes, records, and nonlinear responses. *Earthq Spectra* 14(3):469–500
- Stafford PJ, Berrill JP, Pettinga JR (2009) New predictive equations for Arias intensity from crustal earthquakes in New Zealand. *J Seismol* 13:31–52
- Tarbali K, Bradley BA, Baker JW (2019) Ground motion selection in the near-fault region considering directivity-induced pulse effects. *Earthq Spectra* 35(2):759–786. <https://doi.org/10.1193/102517EQS223M>
- Tiwari AK, Gupta VK (2000) Scaling of ductility and damage-based strength reduction factors for horizontal motions. *Earthquake Eng Struct Dynam* 29(7):969–987
- Travasarou T, Bray JD, Abrahamson NA (2003) Empirical attenuation relationship for Arias intensity. *Earthq Eng Struct Dynam* 32:1133–1155
- Tremblay R (1998) Development of design spectra for long-duration ground motion from Cascadia subduction earthquakes. *Can J Civ Eng* 25:1078–1090

- Vanmarcke EH, Lai SSP (1980) Strong-motion duration and RMS amplitude of earthquake records. *Bull Seismol Soc Am* 70(4):1293–1307
- Yaghmaei-Sabegh S, Shoghian Z, Sheikh MN (2014) A new model for the prediction of earthquake ground-motion duration in Iran. *Nat Hazards* 70(1):69–92
- Zafarani H, Luzi L, Lanzano G, Soghrat M (2018) Empirical equations for the prediction of PGA and pseudo spectral accelerations using Iranian strong-motion data. *J Seismol* 22(1):263–285

Publisher's Note Springer Nature remains neutral with regard to jurisdictional claims in published maps and institutional affiliations.

Springer Nature or its licensor (e.g. a society or other partner) holds exclusive rights to this article under a publishing agreement with the author(s) or other rightsholder(s); author self-archiving of the accepted manuscript version of this article is solely governed by the terms of such publishing agreement and applicable law.